IRAQI JOURNAL OF APPLIED PHYSICS
Vol. 22, No. 1, January-March 2026, pp. 99-108

Effect of Graphene Doping on Structural and Electrical Properties of PAN/PPY Nanocomposites

Bushra A. Hasan [1]
Roaa R. Ahmed [2*]
Ahmad A. Hasan [1]

[1] Department of Physics, College of Science, University of Baghdad, Baghdad, IRAQ
[2] Department of Physics, College of Science, University of Diyala, Diyala, IRAQ
*Corresponding author: ruaa.r@uodiyala.edu.iq

Through chemically polymerizing pyrrole on PAN matrix with $FeCl_3$ as an oxidant, conducting percentage ratios of PPY and PPY have been synthesized. Three distinct percentage changes are made to the PAN/PPY ratio: 90/10, 85/15, and 80/20. By using the polymer approach, the synthesized nanocomposites are characterized. PAN/PPY nanocomposites with doped and undoped graphene have been studied for their electrical conductivity. The frequency dependent AC conductivity indicates that fluctuation in the conductivity regarding the nanocomposites is caused by both graphene doping and the concentration of PPY. It has been discovered that the PPy concentration and Gr doping decreased the nanocomposites' impedance. The results shown that the interfacial space charge (Maxwell Wagner) polarization is responsible for frequency-dependent dielectric constant for various composites at room temperature. Graphene doping is mainly an electronic lever: it tunes carrier density, mobility and inter-flake contact resistance. PPy concentration is mainly a structural lever: it determines whether a continuous conductive polymer network spans the insulating PAN matrix. Thus, in PAN/PPy/graphene composite, the two levers co-operate rather than compete - doped graphene provides fast paths, PPy builds the bridges, and PAN supplies mechanical integrity. The change of dielectric loss as PPY percentage function is provided and analyzed. Frequency-dependent dielectric loss is presented.

Keywords: PAN/PPY nanocomposites; Graphene; FTIR analysis; Cole-Cole diagram; Electrical conductivity
Received: 28 April 2025; Revised: 30 July 2025; Accepted: 6 August 2025; Published: 1 January 2026

1. Introduction

Conducting polymers have good electro chemical, electrical, and optical properties, but their poor processability and stability have limited their popular usage [1]. Due to its excellent thermal and mechanical qualities as well as its affordable price, polyacrylonitrile (PAN) is a superb technical material that is frequently utilized in textile applications [2]. Because of its excellent redox reversibility, outstanding stability, strong electrical conductivity, and relative simplicity of synthesis, polypyrrole (PPy) represents a very significant conducting polymer. Yet, because of its insolubility and extremely fragile structure, PPy has limited practical application. It lacks necessary mechanical characteristics and has poor processability. PPy is a powerful conducting polymer, but too brittle and hard to process on its own. PAN acts as a mechanical backbone, processing aid, and stabilizer, enabling PPy to be used in flexible electronics, sensors, supercapacitors, and wearable devices that would otherwise be impossible using pure PPy [3-5].

The creation of textiles with novel qualities and uses has drawn a lot of interest recently. Textile electrical conductivity is one of such characteristics. Conductive textiles have a wide range of uses, including the decrease of microwave reduction, biomechanical sensors, gas sensors, electrostatic dissipation, heating devices, antistatic applications, and electromagnetic interference shielding, carbon-based conducting polymer nanocomposites have potential applications as electromagnetic interference (EMI) shielding materials owing to their high conductivity and dielectric constant of the materials that contribute to the high EMI shielding efficiency (SE). Because conductive textiles have such favorable microwave absorption properties, they can be utilized in military applications, like radar protective fabrics [6-9]. A variety of solvents, such as dimethyl sulfoxide (DMSO), dimethyl formamide (DMF), toluene, hexane, and methanol, were used in conjunction with azobisisobutyronitrile (AIBN), Ce(IV), benzoyl peroxide (BPO), and the redox system of Ce(IV)–carboxylic acids to achieve chemical polymerization of acrylonitrile to PAN in bulk (with no need for a solvent). DMF, which may form complexes with PAN and has a plasticizing action, is an appropriate solvent for PAN. Individual polymer molecule segments move more freely when DMF is present [10–14]. Electrically conductive composites of PAN–PPy have been created by in situ polymerization of pyrrole on PAN matrix with existence of H_2O_2 and polymer oxidants [15–17]. Via designating PAN as continuous phase (shell) and PPy as dispersed phase (cores), Li et al. [15] have fabricated a core-shell nanostructured conductive composite (core–shell structures by the electrospinning). PAN film pyrrole impregnation was investigated by Lee et al. [16]. A small quantity of a carboxylate (COO) or sulfonate (SO_3^-) group added to the PAN structure increases electrostatic interaction and improves both morphological properties and

electrical conductivity. Poly (acrylonitrile-co-styrene sulfonate) has been employed as matrix by Lee et al. [17] to improve electro-static interaction with polypyrrole. Compared to PAN, anion-containing matrix offered superior stability and electrical conductivity. PAN-PPY composite films were made using the vapor phase approach by Bhat et al. [18]. It was investigated how conductivity changed with $FeCl_3$ content and how polypyrrole uptake coincided with it. Polypyrrole composites were researched by Saafann et al. [19]. The oxidizing agents, ferric chloride and potassium persulphate, demonstrated a noteworthy impact on dielectric characteristics of polypyrrole composites. Polymer composites incorporating polypyrrole/yttrium oxide (PPY/Y_2O_3) have been examined by Vishnuvardhan et al. [20]. The high dielectric constant value at room temperature has been caused by interfacial space charge polarization, also known as Maxwell Wagner polarization. This dielectric constant was frequency dependent. With the use of an *in-situ* deposition approach, Basavraja et al. [21] have fabricated polypyrrole-lead titanate ($PPY/PbTiO_3$) composites. The addition of more $PbTiO_3$ led to higher dielectric constants and dielectric losses, which in turn produced the highest space charge polarization in composites. A review of the literature shows that there are not many in-depth conductivity researches on PAN/PPY composites undoped and doped with graphene, according to carbon-based conducting polymer nanocomposites have potential applications as EMI shielding materials owing to their high conductivity and dielectric constant of the materials that contribute to the high EMI shielding efficiency (SE).

In the present investigation, highly conducting (PAN/PPY)/graphene nanocomposites were prepared by *in-situ* polymerization PAN/PPY with 2% concentration of graphene, we can use different concentration (1%, 3% and 5%) because graphene has remarkable physical, chemical, mechanical, electrical, thermal and microwave absorption properties. In view of the unique structural features of graphene such as its high surface area (theoretical specific surface area (SSA) of 2630 m^2/g), flexibility, high mechanical strength, chemical stability, and superior electric and thermal conductivities, graphene has been considered to be an ideal material for microwave absorption properties. Graphene nanosheets can be viewed as the building unit, and their reassembly provides opportunities to design and prepare specific structures and hybrids with improved properties for different applications [6].

This research examines the characterization, synthesis, and assessment of ac electrical conductivity for various PAN/PPY ratios in both doped and undoped graphene nanocomposites. The Fourier-transform infrared (FTIR) spectroscopy has been utilized to characterize the composites.

2. Experimental Work and Measurements

Chemical polymerization was used to synthesize polypyrrole. Merck provided the pyrrole monomer, which has a melting point of -24 °C and a density of 0.97 g/cm^3 at 20°C. Across Organics provided sodium dodecyl benzene sulfonate (DBSNa), a surfactant with an 88% purity level. From Qrec, iron(III) chloride hexahydrate ($FeCl_3.6H_2O$) was provided as an oxidant. The graphene (Gr) was supplied with a purity level of 98% and a diameter of 6-8 nm. BDH England provided DMSO with a purity level of 99.6%. Impurities at the nanoparticle-polymer interface could act to boost space charge accumulation, which in turn can alter AC/DC conductivity, and where impurities also be affected on dielectric properties. Even the presence of only very small amounts of impurities can have influence on the dielectric constant, dielectric loss and conductivity of nanocomposites. On the other hand, impurities or defects of the polymer-filler interfacial in epoxy/α-Fe_2O_3 nanocomposites can generate additional trapping sites for charge carriers which can reduce the carrier mobility and increase the dielectric loss.

A 3.48 g of DBSNa surfactant was dissolved in 100 cc of distilled water. Another container had 100 cc of pure water mixed with 27.03 g of the oxidant $FeCl_3.6H_2O$. In a 500 mL reaction flask, the solutions were combined and agitated for 15 minutes at two distinct temperatures, namely 0 and 28°C. The choice of temperatures of 0 and 28°C for the preparation of PAN/PPy composites is related to controlling the polymerization mechanism and the properties of the final material. At 0°C (low temperature), the primary goal is to control the polymerization rate and reduce side reactions, since at low temperatures, pyrrole polymerization is slower and more controlled, resulting in the formation of more orderly polymer chains also this temperature provides uniform nanoparticle distribution and reduces agglomeration, this temperature is used when an oxidizer such as $FeCl_3$ is added. The second 28°C temperature which is nearly room temperature was chosen since it represent the normal operating conditions of the materials which help to compare effect of temperature on the reaction rate and polymer structure since, at this temperature, the polarization is faster and may result in different PPy compositions or a different effect on the distribution within the PAN. The solution of 0.15 mol of pyrrole monomer was then dropped gradually into the mixture throughout the course of 240 minutes of reaction time. After filtering and repeatedly washing with distilled water, the resulting black PPy powder was cleaned. At 60°C, this powder has been dried in an oven for 8 hours. To carry out the casting process, the appropriate quantity of PPy and PAN are dissolved in 20 mL of DMF. After transferring the mixture at room temperature for the whole night, it is after that transferred to a plastic Petri dish. Through adding 2%

weight, nano Gr-doped composites have been created. Studying the effect of a specific concentration that can be compared to other studies since many previous studies use ratios between 0.5 and 5% to evaluate the effect of graphene. The 2% is a common choice that facilitates comparison with the scientific literature.

FTIR analysis was used to characterize the composites that were so created. The composites' infrared spectra have been captured in the 4000–450 cm^{-1} range using a Perkin Elmer 1600 IR spectrometer in KBr medium at the room temperature. To improve contact, PAN/PPY doped and undoped with Gr samples were placed in between two electrodes. Hewlett-Packard impedance analyzer 4191A was used to test the electrical resistivity regarding PAN/PPY doped and undoped with Gr composites at room temperature in the frequency range of 1–200 kHz.

3. Results and Discussion

FTIR spectrum of PAN/PPY at various percentage ratios, both doped and undoped with graphene, is displayed in Fig. (1). The PAN film's FTIR–ATR spectrum displays the following peaks: the PAN's C-N stretching as well as C-H bending are represented by bands at 2243 cm^{-1} and 1453 cm^{-1}, respectively. For PAN, peak measured at 2939 cm^{-1} has been a result of the C-H stretching [22–24]. A total of 5 peaks have been seen in PPY FTIR spectrum, and they were situated at 783, 919, 1564, 1710, and 3411 cm^{-1}. The existence of polymerized pyrrole was suggested by the peaks at 783 and 919 cm^{-1} [25]. The peak at 1564 cm^{-1} was in line with the pyrrole ring's typical peak [26]. The formation of COOH groups was indicated by the peak at 1710 cm^{-1}, which correlated with the C=O stretching mode. COOH group's OH stretching mode was identified as the origin of the peak at 3411 cm^{-1} [27]. Gr's FTIR data revealed four distinct peaks. Specifically, they have been at 1269, 1599, 2873, and 3552 cm^{-1}. The C=C backbone stretching as well as the C-N stretching vibrations were responsible for the peaks at 1269 cm^{-1}, respectively [28]. The frequency at 2873 cm^{-1} has been associated with the C-H bond's stretching vibration. OH stretching was consistent with the band at 3552 cm^{-1} [29]. The well pronounced of Graphene peaks C=O appeared at (approximately 1720 cm^{-1}) C–O–C or C–OH (approximately 1050–1250 cm^{-1}) and OH (broad at 3200–3500 cm^{-1}) is ascribed to the double moments of these bonds [30]. The typical C-H and O-H bond peaks are located between 2800 and 3500 cm^{-1}. Those peaks could be linked to groups that are carboxylic and hydroxylic. FTIR spectroscopy was used to examine the impact of pyrrole content on composite films and assess changes in values of absorbance with derivatives of pyrrole. The distinct bands of vibration of PPY ring (C–C stretching) are seen at 1546 cm^{-1}, C–H out of plane vibration at 918–950 cm^{-1}, C–N stretching vibration at 1450 cm^{-1}, and C–H in plane vibration at 1045 and 1310–1316 cm^{-1} [30–36]. PAN-PPy composite films' FTIR spectrum revealed some shift in the absorption bands' positions. The addition of PPy caused absorption band, which was originally located at 1666 cm^{-1}, to shift to 1652 cm^{-1}. It could be the result of an ionic interaction in composite films between the cation-containing PPY (NH group) and anion-containing DMF (C=O group), the bond that connects polypyrrole (PPy) and DMF is mainly ionic and focuses on the Hydrogen bond connection of PPy's N-H group with DMF's C=O moiety. The interaction is hydrogen bonded where PPy NH donates and DMF C=O accepts. This type of bonding greatly affects the structure and electrochemical behavior properties of PAN-PPy composites so that it enhances the solvation of PPy in DMF which increases its dispersion in PAN based solutions [31].

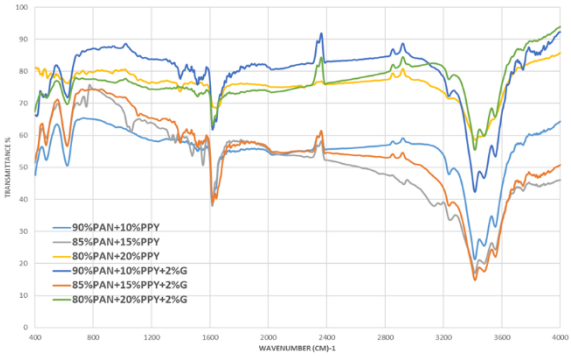

Fig. (1) FTIR spectrum of (PAN/PPY) nanocomposites undoped and doped with graphene

A novel absorption band was observed in composite films at 1318 cm^{-1}, corresponding to CH in the PPY plane vibration peak [28,31,34]. This band's intensity rose as pyrrole was added, showing the integration of PPY into the composite structure. The peak detected at 1453 cm^{-1} is related to PAN's CH bending [37] and produces infrared vibrations when pyrrole is not present. When PPY was added to the PAN solutions, the absorbance of 1453 cm^{-1} significantly increased. The absorption band, which may be seen at 1452 cm^{-1} (1420–1465 cm^{-1}), has previously been identified as PPY's C–N ring stretching [28-31]. Therefore, pyrrole polymerization in the polyacrylonitrile matrix may be the cause of this rise in absorbance.

With the use of Eq. (1) [7], the measured conductance, G(ω), at frequencies ranging from 1 to 200 kHz was utilized to calculate the A.C. electrical conductivity, $\sigma_{ac}(\omega)$:

$$\sigma(\omega) = \frac{G(\omega)d}{A} \qquad (1)$$

where A represents the cross-sectional area and d represents the composite film sample's thickness

Figure (2) displays the AC conductivity of the PAN/PPY nanocomposites both doped and

undoped with graphene at varying mix ratios. The following relation [38] determines the composite films sample's total conductivity, $\sigma_T(\omega)$:

$$\sigma_T(\omega) = \sigma_{dc}(0) + \sigma_{ac}(\omega) = \sigma_{dc}(0) + A\omega^s \quad (2)$$

where

$$(\omega) = \hat{A}\ \omega \quad (3)$$

Â represents a constant based on dosage and frequency exponent s ($s \geq 1$) is represented as [39]:

$$s = \frac{d \ln \sigma}{d \ln \omega} \quad (4)$$

The conductivity versus frequency plot (Fig. 2) of doped nanocomposites samples exhibits 2-step variation; the first step's curve is horizontal and begins at 1k 70 kHz. The mobility regarding bound ions and loosely polarons results in DC (0) conductivity, which is shown by this area of the curve. The second step's rising curves, which show frequency-dependent conductivity caused by bound ions, span frequencies of 70-200 kHz. The PPY binder, whose vibration frequency increases, is primarily responsible for the reaction of bound ions. The study's findings are consistent with previous research [40-43]. In the utilized frequency range, the undoped nanocomposites samples exhibit a single step where the bound ions' frequency-dependent conductivity is represented by rising curves. The AC conductivity (σ_{ac}) curve is usually divided into two distinct regions because there are two types of charge carriers that respond to the applied AC field in two different ways, depending on their relaxation time and the nature of their motion: the first step (1–70 kHz) σ_{dc}: "Plateau" of DC conductivity, the transport mechanism, reason for the constant σ free polarons: which longer range hops between adjacent sites in the material's lattice (hopping) along semiconductor-connected paths. The response time (τ_p) of the polaron exceeded the period of change in this frequency range, so its motion is considered a "DC" (non-frequency dependent). Another contribution named bound ions will slowly hops from one ion trap to another, or partial release from surface binding sites. Here, the response time τ_i is also longer than the signal period, so their contributions appear constant with frequency. The sum of the two motion paths forms a nearly constant "plateau" of σ_{DC}, therefore, the first step will related with the constant conductivity value (σ_0). In the second step (70–200 kHz), the conductivity increases exponentially with (s), $\sigma_{ac} \propto \omega^s$ ($0<s<1$), in this frequency range, ($1/\omega$) becomes smaller than τ_i but still longer than τ_p, or τ_p still relatively slow; it doesn't catch up with the rapid change and appears as only a static conductivity. Its role almost stops at the value of σ_0; it doesn't add a change with frequency. While bound ions jump in a time comparable to $1/\omega$ so it makes short-distance jumps within localized. Thus, the number of jumps per second increases with frequency giving rise to frequency dependent conductivity .The conductivity curve described by Jonscher's universal law: $\sigma(\omega)=\sigma_0+A\omega^s$, where A is a constant that depends on the density and depth of the traps, and s (0–1) relates to the shape of the trap spectrum. The polaron contribution vanish in the second step due to the following reasons:

(i) Electronic/lattice inertia, the polaron involves a local lattice rearrangement around the charge; this "distortion" takes time to form and collapse.in addition at low frequency range $f \geq 70$ kHz, the lattice doesn't have enough time, so the charge appears "heavy" and unable to follow the field core,

(ii) Long-range transport path, it was found the to make the polaron to travel a distance equivalent to a conducting path it needs tens of nanoseconds to microseconds; which is slower than the high-signal period,

(iii) Response is limited to localized jumps, ions, dissimilar polarons, move in very short steps (angstroms) within a local "cage", so they can respond to fields up to hundreds of kilohertz or even megahertz.

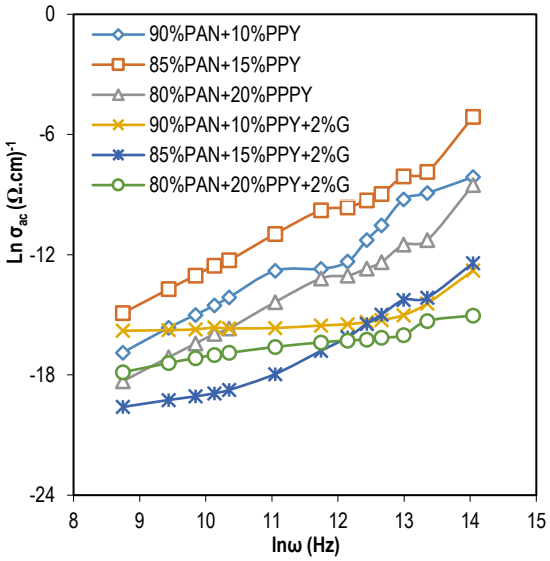

Fig. (2) Variations of Ln σ_{ac} with ln(ω) of (PAN/PPY) nanocomposites undoped and doped with graphene

It can be said that in low frequency range (1–70 kHz), there is quantum combination of extended polaron current + trapped ions which lead to constant conductivity , while in the high frequency range (70–200 kHz) where the polaron stops following; the trapped ions enter a rapid "hop-sequence" phase which leads to frequency dependent conductivity $\sigma_{ac} \propto \omega^s$ [44,45].

The parameter of s, which was determined using Eq. (4), is displayed in table (1). The value of s was determined to follow the power law ($0.376< s < 1.643$). Furthermore, for samples of undoped nanocomposites, the parameter of s obtained has been slightly dependent on the PPY ratio, whereas for samples of doped blends, the parameter was strongly dependent on the PPY ratio. The distinction between undoped and doped samples is

attributed to the distinct mechanisms at play; doping with Gr has the ability to alter the molecules' vibration modes within the samples through phonon-phono interaction [38]. It is evident that (s) values smaller than unity for 90%PAN+10%PPY+2%G samples, which validated the hopping mechanism, and nearly constant and higher than unity for undoped nanocomposites samples and 85%PAN+15%PPY+2%G, 80%PAN+20%PPY+2%G doped blends, which demonstrate that the conductivity is pure AC. Small polaron (SP) models are the most appropriate when (s) increases, whereas small correlated barrier hoping (CBH) models are the most appropriate when (s) drops [46-50], the value of the exponent "s" in determining the type of electrical transport mechanism in materials such as conductive polymers or nanocomposites. Hopping is a mechanism that takes place in insulating or semiconductor materials that are amorphous or contain impurities; electrons do not move easily as they do in metals. Instead, they jump from one local location to another, a transition called "hopping". This process is influenced by the distance between sites and the required energy. The hopping mechanisms, such as Mott hopping and variable range hopping (VRH), in this model the carrier hops between localized states at variable distances and energies, where s is less than 1 and decreases with increasing temperature. Physically, this indicates an enhanced probability of long-range hopping at higher temperatures. The typical range is $0.6<s<1$ (decreasing with T). There are different mechanisms of hopping.

Table (1) Values of PAN/PPY nanocomposites undoped and doped with graphene

Composites sample	s	α
90%PAN+10%PPY	1.635	0.444
85%PAN+15%PPY	1.643	0.277
80%PAN+20%PPY	1.643	0.388
90%PAN+10%PPY+2%G	0.376	0.288
85%PAN+15%PPY+2%G	1.400	0.200
80%PAN+20%PPY+2%G	1.470	0.122

The polarizability (α) values is displayed in table (1). The increase of inter-chain interactions raised polarizability for relaxation effects at greater PPY concentrations. In blends, polymer interfaces can facilitate or impede charge transport and hence alter α, interfacial interactions within the blend. Below a certain threshold of PPY (15% w/w), the matrix could constrain motion of PPY chains which leads to less charge mobility and thus lower polarizability. The oscillatory behavior stems from a delicate balance between a localized dipolarization in the PAN/PPY (decreases with motion isolation) and a broadband interface polarization caused by graphene (increases after the lattice is completed). The surge at 20 wt.% PPY indicates that the PAN/PPY graphene system has reached a "serially connected" capacitor structure, where both polarons and trapped charges are invested at the interface boundaries, resulting in a significant increase in polarizability (α). For further testing of these hypothesis addition measurements (such as spectro-thermal data) required to correlate them with nanoscale morphology images which allows precise composition tuning for applications in integrated capacitors or highly polarized EMI shielding [51].

Complex permittivity was used to investigate the samples' dielectric characteristics, as shown by the following equation:

$$\varepsilon^*(\omega) = \varepsilon'(\omega) + \varepsilon''(\omega) \quad (6)$$

where ε' represents real part of permittivity and ε'' represents imaginary part of permittivity that represents energy storage and energy loss, respectively, in every cycle of applied electric field. The real part $\varepsilon'(\omega)$ has been found according to the following equation:

$$\varepsilon' = (\omega)/A \quad (7)$$

and imaginary part, $\varepsilon''(\omega)$ with the use of the following equation:

$$\varepsilon''(\omega) = \varepsilon'(\omega)\, tan\delta \quad (8)$$

In which, A is sample's surface area, and tan δ represents loss tangent

Plotting ε' and ε'' in figures (3) and (4) makes it clear that the relative permittivity, ε', varies in steps for undoped nanocomposites and in two steps for samples of doped nanocomposites. In step I, there is a clear decrease in ε' for 85/15 PAN/PPY samples compared to 90/10 PAN/PPY samples in frequency range of 1-200 kHz. For 80/20 PAN/PPY samples, there is a subsequent rise in ε'. Doped sample curves in step II are nearly smooth and horizontal in frequency range of 70-200 kHz. In region I, electrode polarization may be the cause of initial high value of ε' (relative permittivity) [51-53]. In contrast, in region II, the drop in ε' is nearly constant throughout frequency range. Since ion diffusion might not be possible in field's direction, this pattern of fluctuation might be caused by periodic reversal of electric field, which happens quickly at high frequency values [51]. Reduced capacitance, C, can lead to dipole alignment with the field and a subsequent decrease in the value of relative permittivity, ε', the permittivity value [54-54]. The variation trend of ε'' in Fig. (4) is comparable to that of ε', meaning that the dielectric loss, ε'', varies in one step for the undoped blend and in two steps for the doped nanocomposites samples.

In the PAN/PPY nanocomposite, the dielectric constant increases with higher content of PPY due to greater polarity and additional dipoles. These effect enhances the material's electrical energy storage capacity, and thus improves in its dielectric properties. Therefore, polypyrrole addition not only elevates the relative permittivity but also enhances other performance characteristics of the nanocomposite for diverse electronic applications. At PAN/PPY interfaces charge carriers such with polarons in PPY form and sustain intermolecular dipole moments. This phenomenon becomes more significant at higher PPY

content due to increased interfacial area which means greater high molecular dipoles when then PPY content is increased [53].

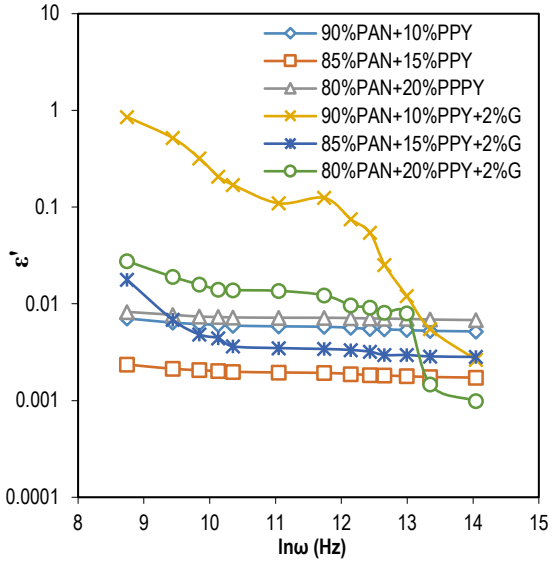

Fig. (3) Variation of ε' with ln(ω) of PAN/PPY nanocomposites undoped and doped with graphene

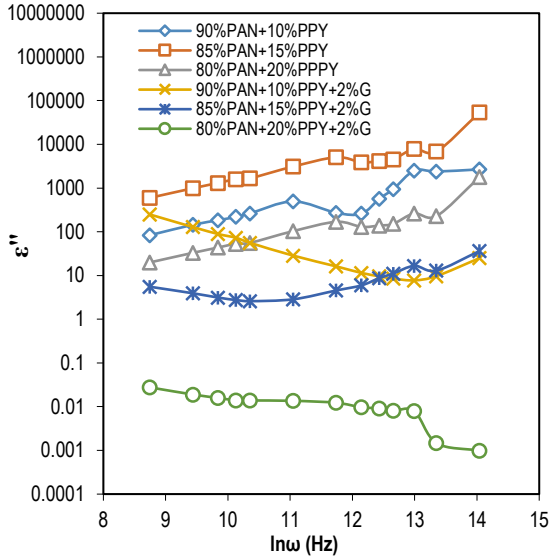

Fig. (4) Variations of ε" with ln(ω) of PAN/PPY nanocomposites undoped and doped with graphene

In step I, it is clear that reduction for doped samples is linear between 1 and 30 kHz in frequency. Curves of step II for every blend ratio are nearly horizontal and smooth, indicating a large loss in "ε" in the 30–200 kHz frequency range. The motion of free charge carriers within materials, which is connected to DC conductivity, could be the cause of the dielectric loss in region I. Mathematically, each step/peak pair corresponds to one dielectric-relaxation time $\tau=1/2\pi f\omega_{ax}$ of a distinct mechanism described well by the Debye- or Havriliak–Negami-type response.

the physical origin of the characteristic range are (i) interfacial (Maxwell–Wagner–Sillars, MWS), here the charge accumulated at interfaces between two phases of very different conductivity/permittivity 10^2-10^6 Hz, (ii) α-relaxation cooperative segmental motion of the polymer matrix (≈glass transition) 10^4–10^8 Hz (strongly T-dependent), and (iii) β/δ-relaxations local dipole flips or side-group rotations 10^6-10^9 Hz. Undoped nanocomposite often shows one step since the material contains the polymer but no highly conductive dopant. Thus, the conductivity contrast between matrix and filler is modest; therefore the MWS interfacial polarization is weak or merges with the intrinsic α-relaxation, i.e., the domination of the α-relaxation of the host polymer one clear step in ε′ and a single loss peak in ε″. It was found that addition of small amount of graphene nanoparticles (GNPs) results in three key effects: first, the introduction of huge conductivity mismatch between graphene (10^4–10^5 S/m) and the insulating matrix and thus a new, low-frequency MWS relaxation appears, (step I in ε′; peak one in ε″). The second is the creation of extra interfacial area and trapped space charge (~10^{10} cm²/cm³ for well-exfoliated flakes) which increases ε′ plateau before the first step and broadens the relaxation time distribution. The third is making percolation-like micro-capacitor network, which lowers the relaxation time (step shifts to lower f) and can split the α-process into two sub-processes (polymer-rich versus graphene-adjacent chains). Therefore, the doped sample displays two sequential drops in ε′ (and two ε″ peaks) [54,55].

As a result, power law dispersion is seen, and the measured frequency range shows no peaks. For pure dielectric materials or non-polar polymers, this peak is easily observed. Conversely, it is noted that samples of undoped nanocomposites exhibit greater relative permittivity values, and that this trend continues to rise with increasing dose. High polarity is the cause of this observation. Consequently, it is thought that the number of dipoles has increased, raising the relative permittivity value.

Cole –Cole Diagram

Direct evidence of existence of multi-relaxation time in PAN/PPY nanocomposites undoped and doped with graphene is obtained through the plotting of Cole–Cole diagrams as can be seen from Fig. (5). It was noted that for all films that have been reported here, ε' versus ε" curves represent the arc of circles that have their centers lying below abscissa axis.

This demonstrates that τ is distributed throughout all of the films. The values of the polarizability (α) have been calculated by measuring angles (απ/2) and were recorded in table (1). It is evident that when the blends ratio increases, the values of α announce an irregular drop. On the other hand, when the PPY ratio rises from 15 to 20 wt.%, α tends to increase. This is consistent with the idea of molecular relaxation; as a barrier forms

between composites, forces decrease, whereas as PPY increases, intermolecular forces rise, values decrease [52-61].

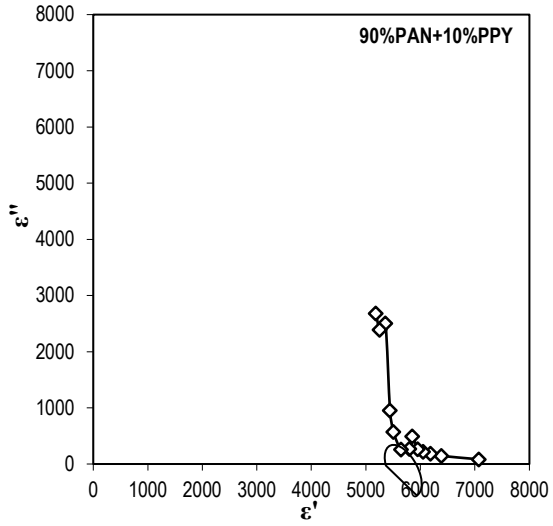

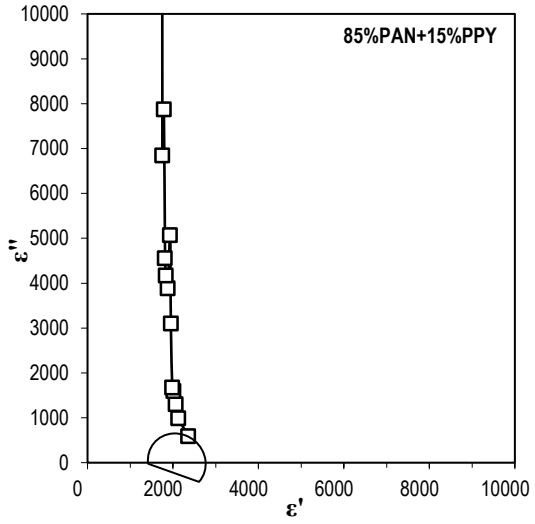

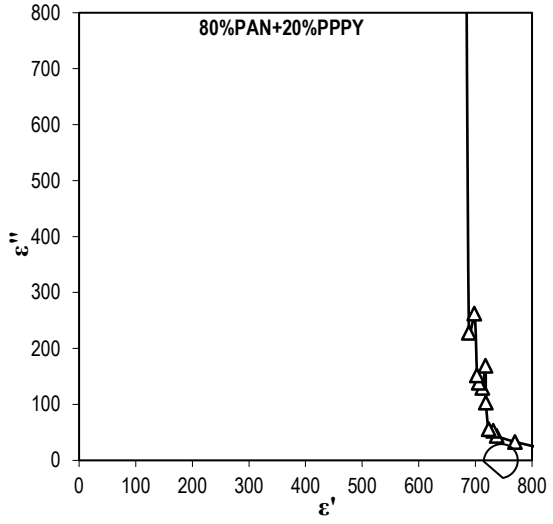

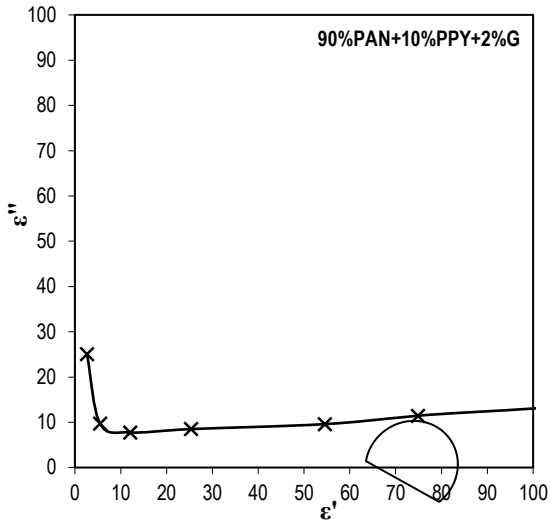

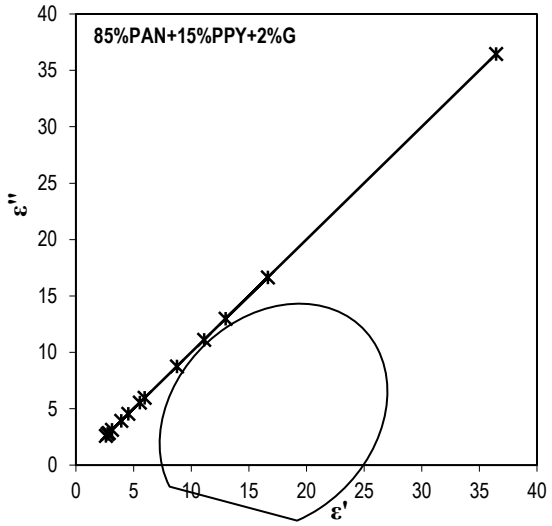

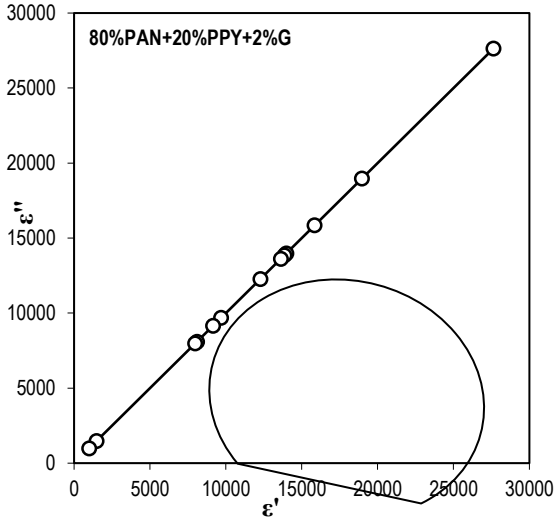

Fig. (5) Relation between ε′ and ε'' of PAN/PPY nanocomposites undoped and doped with graphene

4. Conclusions

From the results obtained from this work, the following conclusions can be presented. Graphene doping introduces a continuous conductive pathway in the polymer matrix, allowing long-range electron transport. This results in frequency-independent (DC) conductivity at low frequencies. In contrast, undoped samples lack such paths and rely solely on localized hopping mechanisms, leading to purely AC conductivity. The relative permittivity and dielectric loss showed weakly dependence upon blends ratio but strongly dependence upon doing with Gr. The variation of PPY blend ratio could be utilized as alternative method for enhancing the conductivity of PAN polymer. The 8–12 wt.% PPY concentration is sufficient for charge-discharging and antistatic coatings, while ~15 wt.% is an ideal balance for flexible electromagnetic shielding and mechanical reliability, on the other hand, 18–25 wt.% is intended for electrochemical or thermal applications that require very high σ, but mechanical endurance and yield are reduced.

References

[1] D. Mecerreyes et al., "Synthesis and characterization of polypyrrole-graft-poly(ε-caprolactone) copolymers: new electrically conductive nanocomposites", *Synth. Met.*, 126 (2002) 173-178.

[2] S.H. Hossein, M. Dabiri and M. Ashrafi, "Chemical and electrochemical synthesis of conducting graft copolymer of acrylonitrile with aniline", *Polym. Int.*, 55 (2006) 1081-1089.

[3] N.G. Sahoo et al., "Polypyrrole coated carbon nanotubes: Synthesis, characterization, and enhanced electrical properties", *Synth. Met.*, 157 (2007) 374-379.

[4] N. Li, D. Shan and H. Xue, "Electrochemical synthesis and characterization of poly(pyrrole-co-tetrahydrofuran) conducting copolymer", *Euro. Polym. J.,* 43 (2007) 2532-2539.

[5] L.M. Yee et al., "Polypyrrole-polyethylene glycol conducting polymer composite films: Preparation and characterization", *Synth. Met.*, 157(8-9) (2007) 386-389.

[6] P.R. Modak, D.A. Nandanwar and S. Kondawar, "Synthesis and Characterisations of Reduced Graphene Oxide Prepared by Microwave Irradiation with Sonication", *J. Phys. Sci.*, 32(2) (2021) 1-13.

[7] P. Lekpittaya et al., "Resistivity of conductive polymer–coated fabric", *J. Appl. Polym. Sci.*, 92(4) (2004) 2629-2636.

[8] H.H. Kuhn, A.D. Child and W.C. Kimbrell, "Toward real applications of conductive polymers", *Synth. Met.*, 71 (1995) 2139-2140.

[9] J.P. Boutrois, R. Jolly and C. Petrescu, "Process of polypyrrole deposit on textile. Product characteristics and applications", *Synth. Met.*, 85 (1997) 1405-1406.

[10] A.S. Sarac et al., "Electroinduced polymerization of acrylonitrile in the presence of Ce(IV)", *J. Polym. Sci. A: Polym. Chem.*, 37(14) (1999) 2319-2327.

[11] A.S. Sarac, B. Ustamehmetoglu and H. Yıldırım, "Electroinduced dispersion polymerization of acrylonitrile in the presence of poly(acrylic acid) and catalytic amount of CE(IV)", *J. Appl. Polym. Sci.*, 84(4) (2002) 723-728.

[12] C. Erbil et al., "Conductometric determination of the end group ionization in acrylamide and acrylonitrile polymers initiated by carboxylic acids", *Euro. Polym. J.,* 30(2) (1994) 149-152.

[13] P. Bajaj, K. Sen and S.H. Bahrami, "Solution polymerization of acrylonitrile with vinyl acids in dimethylformamide", *J. Appl. Polym. Sci.*, 59(10) (1996) 1539-1550.

[14] P.J. Sanchez-Soto et al., "Thermal study of the effect of several solvents on polymerization of acrylonitrile and their subsequent pyrolysis", *J. Anal. Appl. Pyrol.*, 58-59 (2001) 155-172.

[15] X. Li et al., "Fabrication of Polyacrylonitrile/polypyrrole (PAN/Ppy) composite nanofibres and nanospheres with core–shell structures by electrospinning", *Mater. Lett.*, 62(8-9) (2008) 1155-1158.

[16] Y. Lee et al., "Ionic interactions in polyacrylonitrile/polypyrrole conducting polymer composite", *J. Appl. Polym. Sci.*, 69(13) (1998) 2641-2648.

[17] Y. Lee et al., "Electrostatic Interactions in Conducting Polymer Composite PAN/PPy", *Mol. Cryst. Liq. Cryst.*, 316(1) (1998) 313-316.

[18] N.V. Bhat and E. Sundaresan, "Structural and electrical behavior of polyacrylonitrile-polypyrrole composite film", *J. Appl. Polym. Sci.*, 42(6) (1991) 1615-1622.

[19] S.A. Saafan, M.K. El-Nimr and E.H. El-Ghazzawy, "Study of dielectric properties of polypyrrole prepared using two different oxidizing agents", *J. Appl. Polym. Sci.*, 99(6) (2006) 3370-3379.

[20] T.K. Vishnuvardhan et al., "Synthesis, characterization and a.c. conductivity of polypyrrole/Y_2O_3 composites", *Bull. Mater. Sci.,* 29 (2006) 77-83.

[21] C. Basavaraja et al., "Preparation, Characterization and Low Frequency a.c. Conduction of Polypyrrole-Lead Titanate Composites", *Bull. Korean Chem. Soc.*, 28(7) (2007) 1104-1108.

[22] F. Dong et al., "Fabrication of semiconductor nanostructures on the outer surfaces of

polyacrylonitrile nanofibers by in-situ electrospinning", *Mater. Lett.*, 61(11-12) (2007) 2556-2559.

[23] S.H. Goh et al., "Miscibility and specific interactions in polyacrylonitrile/ poly(p-vinylphenol) blends", *Macromol. Rapid Commun.*, 20(3) (1999) 148-151.

[24] Y. Sugahara et al., "Evidence for the Formation of Interlayer Polyacrylonitrile in Kaolinite", *Clays Clay Miner.*, 36 (1988) 343-348.

[25] Y.W. Ju et al., "Electrochemical properties of electrospun PAN/MWCNT carbon nanofibers electrodes coated with polypyrrole", *Electrohimica Acta*, 53 (2008) 5796e803.

[26] H. Mi et al., "Synthesis, characterization and electrochemical behavior of polypyrrole/carbon nanotube composites using organometallic-functionalized carbon nanotubes", *Appl. Surf. Sci.*, 256 (2010) 2284e8.

[27] H.M Park et al., "Electrochemical polymerization of polypyrrole (PPy) andpoly(3-hexylthiophene) (P3HT) using functionalized singlewall carbon nanotubes", *Colloids Surf. A: Physicochem. Eng. Aspects,* 313-314 (2008) 72e6.

[28] Y.S Chen et al., "Gas sensitivity of a composite of multi-walled carbon nanotubes and polypyrrole prepared by vapor phase polymerization", *Carbon,* 45 (2007) 357e63.

[29] S. Konwer and S.K. Dloi, "Synthesis and characterization of polypyrrole/graphite composites and study of their electrical and electrochemical properties", *Mater. Chem. Phys.*, 124 (2010) 738e43.

[30] H. Zhao et al., "Nanostructured polypyrrole/carbon composite as Pt catalyst support for fuel cell applications", *J. Power Sour.,* 184 (2008) 375e80.

[31] T.J. Wen and H.H. Kuo, "The influence of lithium ions on molecular interaction and conductivity of composite electrolyte consisting of TPU and PAN", *J. Sol. State Ion.,* 171(1-2) (2002) 171-180.

[32] L.M. Yee et al., "Preparation and Characterization of Conducting Polymer Composite Films: Polypyrrole and Polyethylene Glycol", *Malay. J. Anal. Sci.*, 11(1) (2007) 133-138.

[33] Q. Cheng et al., "Synthesis and structural properties of polypyrrole/nano-Y2O3 conducting composite", *Appl. Surf. Sci.*, 253(14) (2006) 17361740.

[34] N.V. Bhat, A.P. Gadre and V.A. Bambole, "Thermal analysis of poly(vinylidene fluoride) (PVDF) in composites with polypyrrole (PPy)", *J. Appl. Polym. Sci.*, 54(2) (1994) 201-205.

[35] M. Micusik et al., "Preparation, surface chemistry, and electrical conductivity of novel silicon carbide/polypyrrole composites containing an anionic surfactant", *Polym. Eng. Sci.,* 47(8) (2007) 1198-1206.

[36] L. Al-Mashat et al., "Conductometric Hydrogen Gas Sensor Based on Polypyrrole Nanofibers", *IEEE Sens. J.,* 8(4) (2008) 365-370.

[37] D. Sahin, B. Sarı and H.I. Unal, "An Investigation of Some Parameters on Electrorheological Properties of P ties of Polypyrrole Suspensions ole Suspensions", *Turk. J. Chem.*, 26(1) (2002) 113-124.

[38] H.M. Hamzah, E. Saion and A. Kassim, "AC Conductivity Measurement of PVA-PPY Conducting Polymer Composites", Proc. of 6th Putra Physics Seminar, UPM (2004).

[39] H.M. Hamzah et al., "Temperature Dependence of AC Electrical Conductivity of PVA-PPy-FeCl3 Composite Polymer Films", *Malaysia Polym. J.,* 3(2) (2008) 24-31.

[40] T. Balkan and A.S. Sarac, "Synthesis and characterization of electrically conductive composite films of polypyrrole/poly(acrylonitrile-co-styrene)", *Fiber Polym.*, 12(5) (2011) 565-571.

[41] H.M. Hamzah, "Electrical Properties of Chemically Synthesized PPy Pellets and Polypyrrole and Gamma Ray Induced Polypyrrole Composite Films", MSc thesis, University Putra Malaysia (2006).

[42] N.S. El-Sayed et al., "Development of electrical conducting nanocomposite based on carboxymethyl cellulose hydrogel/silver nanoparticles@polypyrrole", *Synth. Met.,* 250 (2019) 104-114.

[43] O.Gh. Abdullah, Y.A.K. Salman and S.A. Saleem, "Electrical conductivity and dielectric characteristics of in situ prepared PVA/HgS nanocomposite films", *J. Mater. Sci.: Mater. Electron.*, 27(4) (2016) 3591-3598.

[44] D.Stauffer and A. Aharony, **"Introduction to Percolation Theory"**, Taylor & Francis (1994).

[45] T. Rajyalakshmi et al., "Synthesis, characterization and Hall effect studies of highly conductive polyaniline/graphene nanocomposites", *SN Appl. Sci.,* 2 (2020) 530.

[46] B.A. Hasan, D.A. Umran and H.H. Issa, "Fabrication, Structure and Dielectric Properties of Fe_2O_3/MgO Composites", *Nonl. Opt. Quant. Opt.*, 58(1-2) (2023) 73-81.

[47] B.A. Hasan and H.H. Issa, "Dielectric properties and A.C electrical conductivity analysis of $(La_2O_3)_{1-x}(ZnO)_x$", *IOP Conf. Ser.: Mater. Sci. Eng.,* 928 (2020) 072003.

[48] A.A. Hasan, "Dielectric Study of PVC-LiF Composites Films", *Iraqi J. Sci.*, 62(3) (2021) 861-870.

[49] Y.M. Abbas and A.A. Hasan, "Dielectric and gas sensing properties of in situ electrochemically polymerized PPy-MgO-WO_3 nanocomposite films", *Iraqi J. Sci.*, 62(9) (2021) 2915-2933.

[50] B.A. Hasan and A.A. Hasan, "Synthesis and characterization of $(TiO_2)_{1-x}((WO_3)_x$", *Iraqi J. Appl. Phys.*, 20(1) (2024), 117-124.
[51] C. Onuoha, O.O. Onyemaobi and C.N. Anyakwo, "Physical and Morphological Properties of Periwinkle Shell-Filled Recycled Polypropylene Composites", *Int. J. Innov. Sci. Eng. Technol.*, 4(5) (2017) 186-196.
[52] H.N. Najeeb, "Dielectrical and electrical properties of PVA-NaI composites", *Iraqi J. Phys.,* 11(22) (2013) 56-63.
[53] M.R. Kaçal et al., "Evaluation of gamma-ray and neutron attenuation properties of some polymers", *Nucl. Eng. Technol.*, 51(3) (2019) 818-824.
[54] S. Cetiner et al., "PAN/PPY composites films: dielectric, spectroscopic and morphologic characterization", *Fibers Polym.,* 11(6) (2010) 843-850.
[55] M.R. Almafie et al., "Dielectric Properties and Flexibility of Polyacrylonitrile/Graphene Oxide Composite Nanofibers", *ACS Omega*, 7 (2022) 33087-33096.
[56] B.A. Hasan, A.A. Hasan and S.S. Mahmood, "Impact of Zinc Oxide on the Structural and Dielectric Properties of NiO/ZnO Composites", *Int. J. Intelligent Syst. Appl. Eng.*, 11(5s) (2023) 142-149.
[57] A.A. Hasan, "The Role of PU Ratio on the Dielectric Properties of EP/PU Blends", *IOP Conf. Ser.: J. Phy.,* 1032 (2018) 012040.
[58] B.A. Hasan and D.A. Umran, "Dielectric permittivity and ac conductivity of CuInSeTe thin films", *Semicond. Sci. Technol.*, 27 (2012) 125014.
[59] B.A. Hasan, D.A. Umran and M.A. Mankoshi, "Characterization of CuInSTe/CdS Heterojunctions", *IOP Conf. Series: J. Phys.,* 1032 (2018) 012020.
[60] A.A. Hasan, "Synthesis and Dielectric Properties of MgO:ZnO Composites", *Iraqi J. Sci.*, 63(12) (2022) 5232-5241.
[61] B.A. Hasan, H.H. Issa and A.A. Hasan, "Fabrication and Investigation of Structural, Optical and Dielectric Properties of ZnO:MnO_2 Composites", *Iraqi J. Appl. Phys.*, 19(4A) (2023) 21-28.

